Comparison of the electronic structures of $Zn_{1-x}Co_xO$ and $Zn_{1-x}Mg_xO$ nanorods using x-ray absorption and scanning photoelectron microscopies

J. W. Chiou, H. M. Tsai, C. W. Pao, K. P. Krishna Kumar, S. C. Ray, F. Z. Chien, and W. F. Pong[a)]
Department of Physics, Tamkang University, Tamsui, Taiwan 251

M.-H. Tsai
Department of Physics, National Sun Yat-Sen University, Kaohsiung, Taiwan 804

C.-H. Chen and H.-J. Lin
National Synchrotron Radiation Research Center, Hsinchu, Taiwan 300

J. J. Wu, M.-H. Yang, S. C. Liu, and H. H. Chiang
Department of Chemical Engineering, National Cheng Kung University, Tainan, Taiwan 710

C. W. Chen
Department of Materials Science and Engineering, National Taiwan University, Taipei, Taiwan 106

(Received 1 March 2006; accepted 9 June 2006; published online 28 July 2006)

X-ray absorption near-edge structure (XANES) and scanning photoelectron microscopy (SPEM) measurements have been performed for $Zn_{1-x}Co_xO$ and $Zn_{1-x}Mg_xO$ to elucidate the effects of the doping of Co and Mg, which have very different electronegativities, on the electronic structures of ZnO nanorods. The intensities of O *K*-edge near-edge features in the XANES spectra of $Zn_{1-x}Co_xO$ and $Zn_{1-x}Mg_xO$ nanorods are found to be lower than those of ZnO, which suggests that both Co and Mg substitutions of the Zn ions enhance the effective charge on the O ion. The valence-band SPEM measurements show that Mg doping does not increase the density of near-Fermi-level states, which implies that Mg doping will not improve field emission of ZnO nanorods. It is surprising to find that both Co and Mg substitutions of Zn increase the numbers of O 2*p* dominated valence-band states, despite that Co and Mg have larger and smaller electronegativities than that of Zn. © *2006 American Institute of Physics*. [DOI: 10.1063/1.2240108]

II-VI semiconductor zinc oxide (ZnO), which can be tuned by doping with suitable doping elements, has been investigated extensively in recent years because of fundamental and technological importance.[1–5] Diluted magnetic semiconductors (DMSs) such as $Zn_{1-x}Co_xO$ have attracted much interest because it has great potential in future spintronics applications.[6,7] Various studies have been conducted to resolve the controversy concerning the origin of ferromagnetism in DMSs.[8,9] Chiou *et al.* investigated the electronic structure of highly oriented ZnO nanorods using x-ray absorption near-edge structure (XANES) and scanning photoelectron microscopy (SPEM) techniques.[10,11] More recently, Chiou *et al.* suggested that the room-temperature ferromagnetism in $Zn_{1-x}Co_xO$ nanorods is strongly related to the transfer of electrons from *deep* defect states to valence-band Co 3*d* orbitals.[12] On the other hand, the Mg doped $Zn_{1-x}Mg_xO$ nanowires were found to show sensitivity of the band gap with the Mg content, which indicated that this material can be a key material for tunable electronic and optical nanodevices.[13] The microscopic chemical homogeneity of $Zn_{1-x}Mg_xO$ nanostructures was argued to determine the usefulness in their applications.[14] Yang *et al.* demonstrated the potential of ZnO for simple, low-cost applications and showed that the use of $Zn_{1-x}Mg_xO$ alloy reduces the residual *n*-type conductivity associated with defect donor states.[15] Both Co and Mg atoms have two valence *s* electrons; the difference between Co and Mg dopants is the magnetic-property-related extra valence *d* electrons in the Co ions. Since Co has a larger electronegativity (1.88),[16] while Mg has a smaller electronegativity (1.31) than that of Zn (1.65),[16] it is interesting to know the differences in their influence on the electronic properties of ZnO nanorods.

O *K*-, Zn L_3-, Co $L_{3,2}$- and Mg *K*-edges XANES and SPEM spectra were obtained at the National Synchrotron Radiation Research Center (NSRRC) in Hsinchu, Taiwan. Low-temperature chemical vapor deposition was employed to prepare well-aligned $Zn_{1-x}Co_xO$ and $Zn_{1-x}Mg_xO$ nanorods without a catalyst on the Si(100) substrate. Structural characterization of $Zn_{1-x}Co_xO$ and $Zn_{1-x}Mg_xO$ nanorods has been performed using high-resolution transmission electron microscopy (HRTEM). The cross-sectional dark-field images of the nanorods indicate that $Zn_{1-x}Co_xO$ and $Zn_{1-x}Mg_xO$ nanorods have a single-phase structure. HRTEM analyses of the bottom, middle, and top regions of those nanorods show the absence of segregated clusters of impurity phase throughout the nanorods. Details of the preparation are presented elsewhere.[17,18] The size distribution of the nanorods was examined using a scanning electron microscopy (SEM). $Zn_{1-x}Co_xO$ ($x=0$, 0.06, and 0.08) and $Zn_{1-x}Mg_xO$ ($x=0.03$ and 0.10) nanorods were determined to have diameters of 80 ± 20 and 50 ± 10 nm and lengths of 540 ± 50 and 300 ± 50 nm, respectively. These well-aligned nanorods have a hexagonal (wurtzite) structure and are oriented along the ***c*** axis, as shown by the SEM micrographs of the $Zn_{0.92}Co_{0.08}O$ and $Zn_{0.97}Mg_{0.03}O$ nanorods in Figs. 1(a) and 1(b), respectively. Figure 1 displays x-ray diffraction (XRD) measurements of the $Zn_{1-x}Co_xO$ and $Zn_{1-x}Mg_xO$ nanorods and the MgO and CoO powders and the Co- and Mg-metal references. The $Zn_{1-x}Co_xO$ and $Zn_{1-x}Mg_xO$ nanorods have a pre-

[a)]Author to whom correspondence should be addressed; electronic mail: wfpong@mail.tku.edu.tw

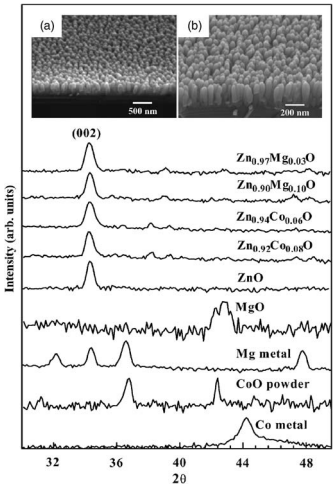

FIG. 1. XRD measurements of the well-aligned $Zn_{1-x}Co_xO$ and $Zn_{1-x}Mg_xO$ nanorods and references MgO, CoO, Co, and Mg metals (on the logarithmic scale). Insets [(a) and (b)] display SEM images of $Zn_{1-x}Co_xO$ ($x=0.08$) and $Zn_{1-x}Mg_xO$ ($x=0.03$) nanorods.

dominant reflection of (002) at ~34°, revealing that Co and/or Mg doping does not change the hexagonal (wurtzite) structure of the ZnO host. The XRD spectra of $Zn_{1-x}Co_xO$ ($Zn_{1-x}Mg_xO$) nanorods did not exhibit any significant characteristic Bragg peak of CoO or Co metal (MgO or Mg metal), which excludes significant CoO (MgO) phase segregation and formation of Co-metal (Mg-metal) clusters/precipitates in the $Zn_{1-x}Co_xO$ ($Zn_{1-x}Mg_xO$) nanorods.

Figure 2 presents normalized O *K*-edge XANES spectra of $Zn_{1-x}Co_xO$ and $Zn_{1-x}Mg_xO$ nanorods. Features A_1-E_1 of $Zn_{1-x}Co_xO$ and $Zn_{1-x}Mg_xO$ are attributable to electron transition from O 1*s* to $2p_\sigma$ (along the bilayer) and O $2p_\pi$ (along the ***c*** axis) states.[10,11] The fact that the intensities of these features are lower than those of ZnO (clearly seen in the upper inset) shows that the number of unoccupied O 2*p*-derived states is reduced, which can be interpreted as transfer of electrons from Co and Mg dopants to O 2*p* states due to O 2*p*–Co 3*d* and O 2*p*–Mg 3*sp* hybridizations in $Zn_{1-x}Co_xO$ and $Zn_{1-x}Mg_xO$ nanorods, respectively. The assignment of hybridization between O and Mg atoms in $Zn_{1-x}Mg_xO$ nanorods is inferred from first-principles pseudopotential calculations for bulk $Zn_{1-x}Mg_xO$ with the local-density approximation; details of the computation are presented elsewhere.[19] The upper inset clearly shows that the decrease of the intensities of features A_1 and B_1 in $Zn_{1-x}Co_xO$ exceeds those of $Zn_{1-x}Mg_xO$. The inset also shows that the intensities of these features decrease roughly linear with the increase of the Co concentration for $Zn_{1-x}Co_xO$ nanorods. As for $Zn_{1-x}Mg_xO$ nanorods, the decrease of the intensities of features A_1 and B_1 tends to saturate especially for feature A_1. The decrease of the O *K*-edge XANES intensity implies an increase of the O 2*p*-orbital occupation or the negative effective charge on the O ions. The increase of the effective charge of the O ion by Mg doping is understandable because Mg has a much lower electronegativity than that of Zn (1.31 vs 1.65),[16] which decreases the average electronegativity of cations. However, Co has a larger electronegativity than that of Zn (1.88 vs 1.65);[16] the increase of the effective charge of the O ions may be due to that the O 2*p* and Co 3*d* hybridizations lowers the energies of O 2*p* orbitals. The lower inset in Fig. 2 displays the normalized Zn L_3-edge XANES spectra of $Zn_{1-x}Co_xO$ and $Zn_{1-x}Mg_xO$ nanorods. The intensity of the Zn L_3-edge near-edge features in $Zn_{1-x}Co_xO$ and $Zn_{1-x}Mg_xO$ nanorods, which are associated with transition of electrons from Zn 2*p* states to unoccupied Zn 4*s*3*d* states,[10,11] increases noticeably relative to that of the ZnO host for $Zn_{1-x}Co_xO$, which indicates a slight decrease of the electron charge on Zn ions and may be due to the loss of a small fraction of its electrons to Co ions because Co has a larger electronegativity. However, it is not clear why the intensities are insensitive to Mg doping, despite a much smaller electronegativity of Mg.

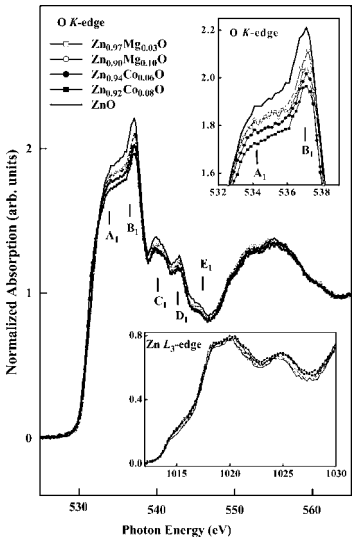

FIG. 2. Normalized O *K*-edge XANES spectra of $Zn_{1-x}Co_xO$ and $Zn_{1-x}Mg_xO$ nanorods. The upper inset shows magnified view of A_1 and B_1 features of the $Zn_{1-x}Co_xO$ and $Zn_{1-x}Mg_xO$ nanorods. The lower inset presents normalized Zn L_3-edge spectra of $Zn_{1-x}Co_xO$ and $Zn_{1-x}Mg_xO$ nanorods.

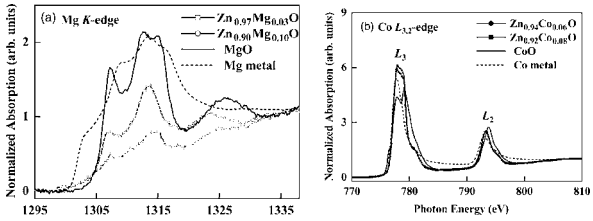

FIG. 3. (a) Normalized Mg *K*-edge XANES spectra of $Zn_{1-x}Mg_xO$ nanorods, MgO, and Mg metal. (b) shows Co $L_{3,2}$-edge spectra of $Zn_{1-x}Co_xO$ nanorods, CoO, and Co metal.

Figure 3(a) presents normalized Mg *K*-edge XANES spectra of $Zn_{1-x}Mg_xO$ nanorods, MgO, and Mg metal. Spectral line shapes of the Mg metal clearly differ from those of the $Zn_{1-x}Mg_xO$ and MgO samples. According to the dipole transition selection rule, the main near-edge features of $Zn_{1-x}Mg_xO$ are associated primarily with transition of electrons from Mg 1*s* to 3*p* unoccupied states. The intensities of these features clearly increase with x for $Zn_{1-x}Mg_xO$ nanorods. Since the shapes of these features are similar to those of MgO, the dependence of the intensities on x suggests that the increase of the number of unoccupied Mg 3*p*-derived states with x is due to increased Mg 3*p*–O 2*p* hybridization. Figure 3(b) presents normalized Co $L_{3,2}$-edge XANES spectra of $Zn_{1-x}Co_xO$ nanorods, CoO, and Co metal, for transition of electrons from Co $2p_{3/2}$ (L_3) and $2p_{1/2}$ (L_2) states to unoccupied Co 3*d* and 4*s* states. The general line shapes of the Co $L_{3,2}$-edge XANES spectra of the $Zn_{1-x}Co_xO$ nanorods are similar to those of polycrystalline $Zn_{1-x}Co_xO$ bulk/film,[20,21]

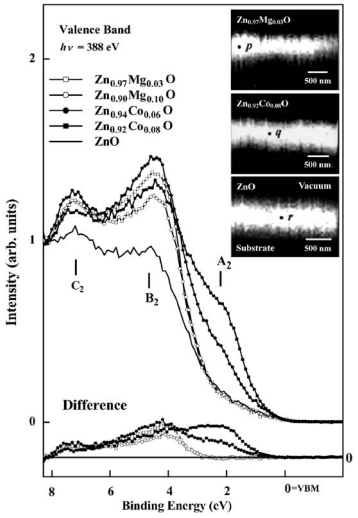

FIG. 4. Valence-band photoemission spectra obtained from selected positions ***p***, ***q***, and ***r*** shown in the upper inset, which present the Zn 3*d* SPEM cross-sectional images of the well-aligned $Zn_{1-x}Mg_xO$ ($x=0.03$), $Zn_{1-x}Co_xO$ ($x=0.08$), and ZnO nanorods. The lower inset shows the difference valence-band spectra of $Zn_{1-x}Co_xO$ and $Zn_{1-x}Mg_xO$ with respect to ZnO nanorods.

but differ clearly from those of CoO and the Co metal.

Figure 4 displays spatially resolved valence-band photoemission spectra of $Zn_{1-x}Co_xO$ and $Zn_{1-x}Mg_xO$ nanorods. The upper inset in the figure shows the Zn 3*d* SPEM cross-sectional images of the selected nanorods for $x=0.03$ $Zn_{1-x}Mg_xO$, $x=0.08$ $Zn_{1-x}Co_xO$, and pure ZnO, respectively. The bright areas in the SPEM images correspond to the nanorods with the maximum Zn 3*d* intensity. The valence-band photoemission spectra presented in Fig. 4 shows the photoelectron yields from sidewall regions ***p***, ***q***, and ***r*** in respective nanorods. The zero energy refers to the valence-band maximum (VBM), which is the threshold of the emission spectrum and is also the Fermi level (E_f). The prominent feature at ~4.5 eV (feature B_2) in the spectra is dominated by the occupied O 2*p* states and that at ~7.3 eV (feature C_2) is associated with the O 2*p* and Zn 3*d*/4*sp* hybridized states of the ZnO nanorods.[10,11] The figure shows that the intensities of these two features for $Zn_{1-x}Co_xO$ and $Zn_{1-x}Mg_xO$ increase with x. A shoulder (feature A_2) centered at ~2.2 eV below VBM exists for $Zn_{1-x}Co_xO$ ($x\neq 0$) nanorods, but is absent for $Zn_{1-x}Mg_xO$, which indicates that it is associated with the Co 3*d* partial density of states (DOS).[20,21] Near the bottom of Fig. 4 shows the difference valence-band spectra of $Zn_{1-x}Co_xO$ and $Zn_{1-x}Mg_xO$ relative to that of ZnO nanorods, which are attributable to Co 3*d* and 4*sp* and Mg 3*sp* DOSs for $Zn_{1-x}Co_xO$ and $Zn_{1-x}Mg_xO$ (Ref. 19) nanorods, respectively. The intensity of feature A_2 increases with the Co concentration, which provides an evidence of the presence of Co 3*d* states near/below the VBM for $Zn_{1-x}Co_xO$. The theoretical calculations of Sato and Katayama-Yoshida correlated the ferromagnetism in $Zn_{1-x}Co_xO$ nanorods with a high DOS of Co 3*d* minority-spin states at/near E_f.[22] Chiou *et al.*[12] suggested that ferromagnetism in $Zn_{1-x}Co_xO$ nanorods is related to the coupling between Co 3*d* moments and deep defect states near/below VBM or E_f, which induces ferromagnetic spin-spin interactions between Co atoms. Note that the *n*-type deep defect states, such as oxygen vacancies, are readily present in naturally grown ZnO.[23] Defects have been argued to tend to form bound magnetic polarons that coupled with the Co 3*d* spin moments within its orbits, and the overlap of two similar magnetic polarons has been argued to cause spin-spin interactions between Co ions,[24] which stabilize ferromagnetic ordering in $Zn_{1-x}Co_xO$ nanorods. The present SPEM result shows that both Co and Mg dopings enhance the numbers of occupied states, despite that one has a larger and another has a smaller electronegativity than the substituted Zn. However, the Mg doping does not increase the density of near-VBM (or E_f) states, which contributes to the field emission of the highly aligned ZnO nanorods. Thus, as the field-emission application is concerned, Mg doping does not offer any merit to enhance the relevant density of near-VBM (or E_F) states in agreement with the results of direct measurements of field emissions for ZnMgO and ZnO nanowires by Lee *et al.*[25]

[1] A. Tsukazaki, A. Ohtomo, T. Onuma, M. Ohtani, T. Makino, M. Sumiya, K. Ohtani, S. F. Chichibu, S. Fuke, Y. Segawa, H. Ohno, H. Koinuma, and M. Kawasaki, Nat. Mater. **4**, 42 (2005), and references therein.
[2] J.-K. Lee, M. Nastasi, D. W. Hamby, and D. A. Lucca, Appl. Phys. Lett. **86**, 171102 (2005).
[3] S. Y. Bae, H. C. Choi, C. W. Na, and J. Park, Appl. Phys. Lett. **86**, 033102 (2005).
[4] M. Gabas, S. Gota, J. R. Ramos-Barrado, M. Sanchez, N. T. Barrett, J. Avila, and M. Sacchi, Appl. Phys. Lett. **86**, 042104 (2005).
[5] M. Losurdo and M. M. Giangregorio, Appl. Phys. Lett. **86**, 091901 (2005).
[6] H. Ohno, Science **281**, 951 (1998).
[7] T. Dietl, H. Ohno, F. Matsukura, J. Cibert, and D. Ferrand, Science **287**, 1019 (2000).
[8] J.-Y. Kim, J.-H. Park, B.-G. Park, H.-J. Noh, S.-J. Oh, J. S. Yang, D.-H. Kim, S. D. Bu, T.-W Noh, H.-J. Lin, H.-H. Hsieh, and C. T. Chen, Phys. Rev. Lett. **90**, 017401 (2003).
[9] P. V. Radovanovic and D. R. Gamelin, Phys. Rev. Lett. **91**, 157202 (2003).
[10] J. W. Chiou, J. C. Jan, H. M. Tsai, C. W. Bao, W. F. Pong, M.-H. Tsai, I.-H. Hong, R. Klauser, J. F. Lee, J. J. Wu, and S. C. Liu, Appl. Phys. Lett. **84**, 3462 (2004).
[11] J. W. Chiou, K. P. Krishna Kumar, J. C. Jan, H. M. Tsai, C. W. Bao, W. F. Pong, F. Z. Chien, M.-H. Tsai, I.-H. Hong, R. Klauser, J. F. Lee, J. J. Wu, and S. C. Liu, Appl. Phys. Lett. **85**, 3220 (2004).
[12] J. W. Chiou, W. F. Pong, M.-H. Tsai, J. J. Wu, I.-H. Hong, C.-H. Chen, H.-J. Lin, and J. F. Lee, National Synchrotron Radiation Research Center Activity Report 2004/2005.
[13] T. Makino, Y. Segawa, M. Kawasaki, A. Ohtomo, R. Shiroki, K. Tamura, T. Yasuda, and H. Koinuma, Appl. Phys. Lett. **78**, 1237 (2001).
[14] M. Lorenz, E. M. Kaidashev, A. Rahm, Th. Nobis, J. Lenzner, G. Wagner, D. Spemann, H. Hochmuth, and M. Grundmann, Appl. Phys. Lett. **86**, 143113 (2005).
[15] H. Yang, Y. Li, D. P. Norton, S. J. Pearton, S. Jung, F. Ren, and L. A. Boatner, Appl. Phys. Lett. **86**, 172103 (2005).
[16] *Table of Periodic Properties of the Elements* (Sargent-Welch Scientific, Skokie, IL, 1980).
[17] C.-H. Ku, H.-H. Chiang, and J. J. Wu, Chem. Phys. Lett. **404**, 132 (2005).
[18] J. J. Wu and S. C. Liu, Adv. Mater. (Weinheim, Ger.) **14**, 215 (2002); J. J. Wu, S. C. Liu, and M. H. Yang, Appl. Phys. Lett. **85**, 1027 (2004).
[19] C. W. Chen (unpublished).
[20] S. C. Wi, J.-S. Kang, J. H. Kim, S.-B. Cho, B. J. Kim, S. Yoon, B. J. Suh, S. W. Han, K. H. Kim, K. J. Kim, B. S. Kim, H. J. Song, H. J. Shin, J. H. Shim, and B. I. Min, Appl. Phys. Lett. **84**, 4233 (2004).
[21] M. Kobayashi, Y. Ishida, J. I. Hwang, T. Mizokawa, A. Fujimori, K. Mamiya, J. Okamoto, Y. Takeda, T. Okane, Y. Saitoh, Y. Muramatsu, A. Tanaka, H. Saeki, H. Tabata, and T. Kawai, Phys. Rev. B **72**, 201201 (2005).
[22] K. Sato and H. Katayama-Yoshida, Jpn. J. Appl. Phys., Part 2 **40**, L334 (2001).
[23] N. E. Hsu, W. K. Hung, and Y. F. Chen, J. Appl. Phys. **96**, 4671 (2004).
[24] M. Venkatesan, C. B. Fitzgerald, J. G. Lunney, and J. M. D. Coey, Phys. Rev. Lett. **93**, 177206 (2004); J. M. D. Coey, M. Venkatesan, and C. B. Fitzgerald, Nat. Mater. **4**, 173 (2005).
[25] C. Y. Lee, T. Y. Tseng, S. Y. Li, and P. Lin, Nanotechnology **16**, 1105 (2005).